

# Searches and Prospects for Standard Model Higgs boson at the Tevatron

Gregorio Bernardi

LPNHE-Paris, Universities of Paris 6 and 7, France

on behalf of the CDF and DØ Collaborations

We report on results obtained at the Tevatron by the CDF and DØ collaborations up to June 2008 ( $2.4 \text{ fb}^{-1}$ ), on searches for standard model (SM) Higgs bosons having a high mass (135-200 GeV). High mass Higgs bosons decay dominantly in  $WW^*$  and the presented searches are performed in the leptonic decay modes of the  $W$ 's. Both direct production ( $p\bar{p} \rightarrow H$ ) and associated production ( $p\bar{p} \rightarrow WH$ ) are studied and eventually combined with all channels available at the Tevatron. Prospects for SM Higgs searches with the full projected Tevatron statistics are also given.

## 1. INTRODUCTION

The Tevatron experiments are searching for the standard model (SM) Higgs boson which is expected to be the footprint of the spontaneous breaking of the electroweak symmetry. This mechanism provides an explanation for the masses of the elementary particles, which are massless in the unbroken gauge theory, so experimental confirmation is eagerly awaited for. Direct searches at LEP have constrained its mass to be above 114.4 GeV [1] while indirect searches constrain it to be below 190 GeV, when taking into account the direct bound [2]. We report here on the searches at high mass (defined as the searches in which the Higgs boson decays in a pair of  $W$ 's) while the low mass analyses are described in another contribution to this conference [3]. For Higgs boson searches, at "high" mass (135-200 GeV), the most sensitive production channel at the Tevatron (center-of-mass energy of  $\sqrt{s} = 1.96 \text{ TeV}$ ) is the direct production ( $p\bar{p} \rightarrow H$ ), but all possible channels are studied to gain sensitivity through their combination, in particular associated Higgs-electroweak boson production ( $p\bar{p} \rightarrow WH, ZH$ ).

In this report, we first describe briefly the  $WH$  analyses, which have lower sensitivity at high mass, then report in more details on the  $H \rightarrow WW$  analyses. We then present the combination of these results with those obtained on searches for low mass Higgs and conclude with the prospects on SM Higgs boson search at the Tevatron.

## 2. SEARCH FOR $p\bar{p} \rightarrow WH \rightarrow WWW$

The search for  $p\bar{p} \rightarrow WH \rightarrow WWW$  relies on the search for two leptons having the same electric charge (in this report, "lepton" refers to electron,  $e$ , or muon,  $\mu$ ). No explicit requirements are put on the decay of the third  $W$  produced, and the like-sign condition ensures orthogonality with the  $p\bar{p} \rightarrow H \rightarrow WW$  searches, described below.

At CDF, a new analysis with  $1.9 \text{ fb}^{-1}$  has recently been presented [4]. For the event selection the requirements are: at least one electron with  $E_T > 20 \text{ GeV}$  and  $p_T > 10 \text{ GeV}$  or one muon with  $p_T > 20 \text{ GeV}$ , and at least one other electron with  $E_T > 6 \text{ GeV}$  and  $p_T > 6 \text{ GeV}$  or one muon with  $p_T > 6 \text{ GeV}$ . Other lepton selection requirements include isolation, track quality, and the consistency of detector response with expectations for electrons or muons. Photon conversion resulting in electron candidates are rejected by identifying an oppositely charged track satisfying a conversion configuration. For the events containing exactly two leptons passing the lepton selection, the two leptons must originate from the same event vertex, satisfy a di-lepton mass selection of ( $M_{ll} > 12 \text{ GeV}$ ) and a  $Z$ -event veto.

The remaining background can be classified in two types, "physics" and "instrumental". Backgrounds containing prompt real leptons (physics backgrounds) are estimated using simulated samples. Such backgrounds can be further classified into reducible (Drell-Yan,  $W$ +heavy flavor hadrons,  $t\bar{t}$ , and  $WW$ ), and irreducible ( $WZ, ZZ$ ). Instrumental backgrounds include residual photon-conversion events which are one of the dominant backgrounds for such like-sign

di-lepton analysis. Such background is determined from the data and the simulation [4]. Other types of fake lepton events are also an important source of background, for instance the overlap of a charged and a neutral pion, or the misidentification of a charged pion into a muon. Their estimation is described in detail in [4]. For the final selection the like-sign di-lepton events are examined on the two dimensional plane of the  $2^{nd}$  lepton  $p_T$  ( $p_{T2}$ ) vs the di-lepton system  $p_T$  ( $p_{T12}$ ). In the most sensitive region,  $p_{T2} > 20$  GeV and  $p_{T12} > 15$  GeV, 3 events are observed, while 3.2 background events and 0.2 Higgs events are expected, if  $m_H = 160$  GeV. No significant discrepancies are found between the data and the background expectations and so four regions are selected in this plane from which the limits are extracted and then combined.

The  $D\mathcal{O}$  collaboration did not update its 2007 result based on  $1.1 \text{ fb}^{-1}$ . The selection was similar to the one described above for the recent CDF result, and the instrumental background is also determined from the data but with a different technique [5]. An important difference with the CDF analysis comes from the limit determination which in the case of  $D\mathcal{O}$  was set using the results of a topological likelihood discriminant [6] resulting in limits of comparable sensitivity, as shown in figures 1. These limits are still a factor of about 20 above the standard model prediction for  $m_H = 160$  GeV, but are more sensitive at low mass if one assumes fermiophobic models.

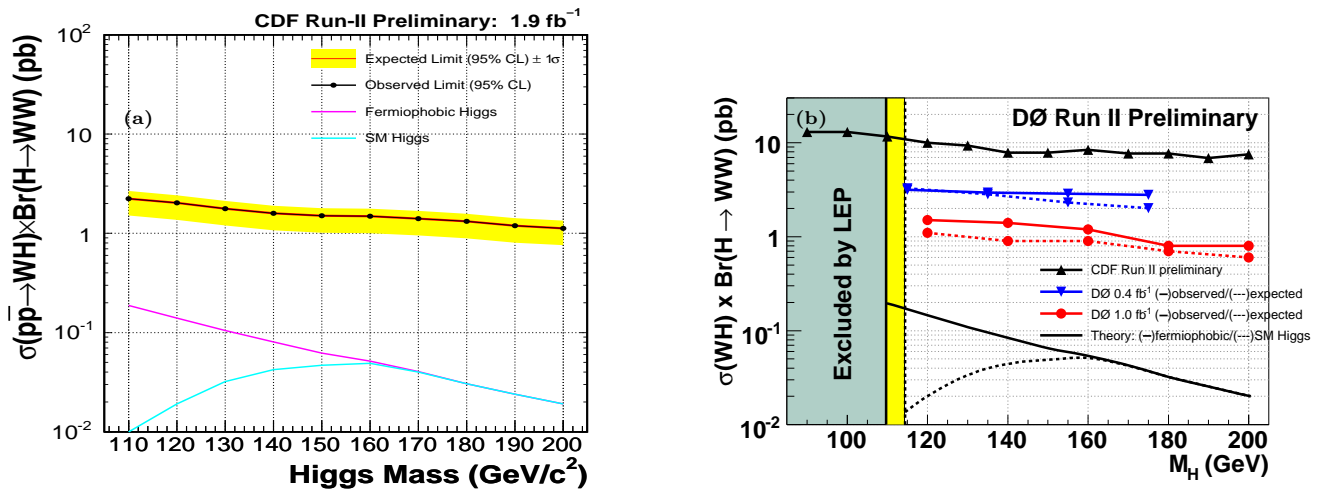


Figure 1: 95% C.L. limits on  $WH \rightarrow WW$  production cross section, as obtained by CDF and  $D\mathcal{O}$

### 3. SEARCH FOR $p\bar{p} \rightarrow H \rightarrow WW$

The most sensitive channel at high mass is by far  $p\bar{p} \rightarrow H \rightarrow WW$ , where production can be via gluon-gluon or vector-boson fusion. Both CDF and  $D\mathcal{O}$  have updated their previous results, and are using  $2.4$  and  $2.3 \text{ fb}^{-1}$  respectively. We first describe the individual analysis, then their combination.

#### 3.1. $D\mathcal{O}$ Results on $p\bar{p} \rightarrow H \rightarrow WW$

The  $H \rightarrow WW$  candidates are selected by triggering on single or di-lepton events with approximately 100% efficiency for the events of the final selection [7]. In the offline selection, electrons must be reconstructed within a detector pseudorapidity  $|\eta| < 3.0$ . Muons are required to be in the fiducial coverage of the muon system  $|\eta| < 2.0$ . The two leptons must originate from the same primary vertex and are required to be of opposite charge. They must have  $p_T^e > 20$  GeV for the leading electron and  $p_T^e > 15$  GeV for the trailing one in the  $ee$  channel,  $p_T^e > 15$  GeV

for the electron and  $p_T^\mu > 10$  GeV for the muon in the  $e\mu$  final state and  $p_T^\mu > 10$  GeV for the leading and trailing muons in the  $\mu\mu$  final state. The di-lepton invariant mass must also be greater than 15 GeV.

At this “pre-selection” stage, the background is dominated by  $Z/\gamma^*$  production which is suppressed by requiring missing transverse energy and scaled missing transverse energy [7]:  $Z/\gamma^*$ , di-boson and multi-jet events are also rejected with a cut on the opening azimuthal angle  $\Delta\varphi_{\ell\ell}$ , since most of the background decays are back-to-back which is not the case for Higgs boson decays because of the spin correlations induced by its scalar nature.  $t\bar{t}$  events are further rejected by a cut on  $H_T$ , the scalar sum of the  $p_T$  of good jets in the event.

The signal and SM background processes are simulated with PYTHIA [8] (except for  $W/Z$ +jets in the  $\mu\mu$  channel, where ALPGEN [9] is used) using the CTEQ6.1M [10] parton distribution functions. The  $Z/\gamma^* \rightarrow \ell\ell$  cross section is calculated at NNLO [11] with CTEQ6.1M PDFs. The NLO  $WW$ ,  $WZ$  and  $ZZ$  production cross section values are taken from [12]. The background due to multijet production, when jets are misidentified as leptons, is determined from the data. See [7] for more details and for the simulation of the other backgrounds.

Additional Higgs mass and final-state dependent selections are optimized to further suppress contributions from  $Z/\gamma^*$ , di-boson ( $WW, WZ, ZZ$ ),  $W(\rightarrow \ell\nu) + jets$ , and multijet backgrounds. Table I shows the number of expected and observed events after pre-selection and final selections (i.e. NN input stage), for all three channels.

	$ee$ pre-selection	$ee$ final	$e\mu$ pre-selection	$e\mu$ final	$\mu\mu$ pre-selection	$\mu\mu$ final
Signal ( $m_H = 160$ GeV)	$1.34 \pm 0.03$	$0.82 \pm 0.02$	$3.58 \pm 0.05$	$1.76 \pm 0.04$	$3.52 \pm 0.08$	$2.08 \pm 0.03$
Total Background	$49306 \pm 306$	$10.7 \pm 1.7 \pm 1.7$	$1436 \pm 138$	$21.1 \pm 1.3 \pm 3.4$	$110681 \pm 231$	$831.8 \pm 29 \pm 34$
Data	50593	10	1424	18	109918	839

Table I: Expected and observed number of events in each channel after pre-selection and final selections (NN input stage). Statistical and systematic uncertainties in the expected yields are shown for the final backgrounds.

In the  $ee$  and  $e\mu$  channels, the signal-to-background is about 10%. In the  $\mu\mu$  channel it is significantly lower, since the cuts have been relaxed on purpose to increase the signal acceptance. In these three cases, multivariate techniques are then applied to enhance the signal. Neural networks (NN’s) are used in each of the three channels. and are trained separately for each Higgs boson mass tested. In the  $\mu\mu$  channel, a weighted sum of all backgrounds is used for the training while for the  $ee$  and  $e\mu$  channels the NN is trained only against the main  $W + jets$  and  $WW$  backgrounds. Input variables to the NN’s are derived based on the separation power of the various distributions, for each of the three channels. They fall into three classes: object kinematics, event kinematics and angular variables, see [7] for the complete list. One of the crucial input variables is a discriminant constructed using the Matrix Element (ME) method, in which Leading-order parton states for either signal ( $H \rightarrow WW$ ) or  $WW$  background are integrated over to find the probability that the event is signal- or background-like. The NN output for  $m_H = 160$  GeV is displayed at preselection level and at final selection level in Figures 2c,d and 3a,b for the  $ee$  and  $e\mu$  channels, respectively, and in Figure 2a,b the corresponding ME output is shown. In Figure 4 are shown the ME discriminant and the NN output of the  $\mu\mu$  channel at the final selection level.

The expected number of background and signal events depend on efficiencies that lead to the systematic uncertainties detailed in [7]. The total uncertainty on the background is approximately 16% and 10% on the signal efficiency. After all selection cuts, the sum of the expected backgrounds describe properly the NN output distributions, which are used to set limits on the production cross section times branching ratio  $\sigma \times BR(H \rightarrow WW^{(*)})$ . Limits are determined for each channel using the CLs method with a log-likelihood ratio (LLR) test statistic [13] and are then combined. To minimize the effects of systematic uncertainties, the background contributions are fitted to the data observation by maximizing a profile likelihood function assuming the presence or the absence of signal [14]. Table II presents the expected and observed combined upper limits at 95% CL for  $\sigma \times BR(H \rightarrow WW^{(*)})$  relative to that expected in the SM for each Higgs boson mass considered. Figure 7a displays the expected and observed limits for  $\sigma \times BR(H \rightarrow WW^{(*)})$  relative to the SM for the different Higgs boson masses for the current Run II dataset of  $2.3 \text{ fb}^{-1}$  analyzed by  $D\mathcal{O}$ .

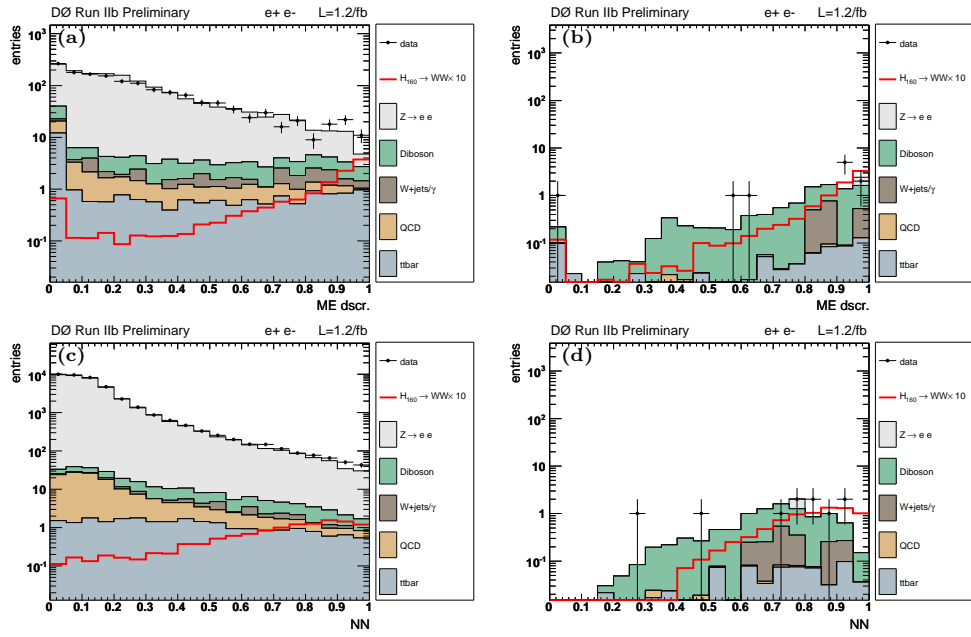


Figure 2: Distribution of the ME and NN output in the  $D\bar{O}$   $ee$  analysis at the preselection (a and c) and at final selection level (b and d), in the Run IIb ( $1.2 \text{ fb}^{-1}$ ) subsample. The distributions of a different NN output using a smaller set of input variables and without using the ME discriminant, trained on the Run IIa subsamples are shown in [15].

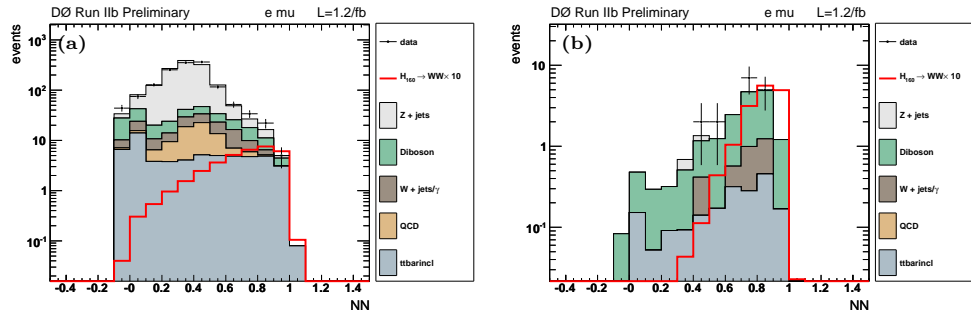


Figure 3: Distribution of the NN output in the  $D\bar{O}$   $e\mu$  analysis at the preselection (a) and final selection (b) level, in the Run IIb ( $1.2 \text{ fb}^{-1}$ ) subsample. For the distributions of the different NN output used in Run IIa, see [15].

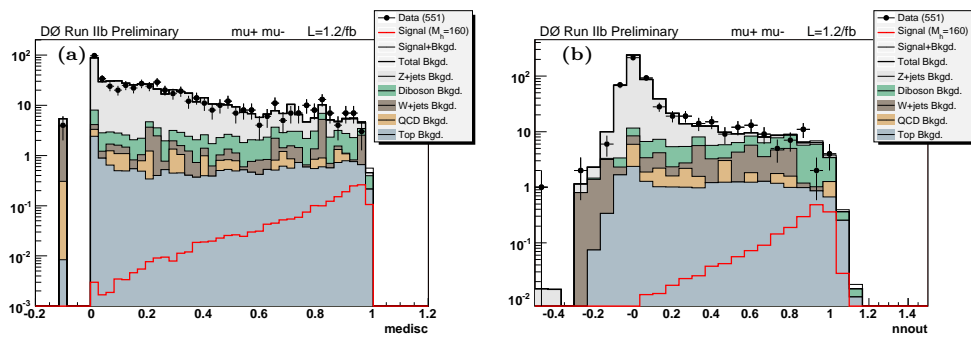


Figure 4: Distribution of the ME (a) and NN (b) output in the  $D\bar{O}$   $\mu\mu$  analysis at the final selection level, in the Run IIb ( $1.2 \text{ fb}^{-1}$ ) subsample. For the distributions of the different NN output used in Run IIa, see [15].

Table II: Expected and observed upper limits at 95% CL for  $\sigma \times BR(H \rightarrow WW^{(*)})$  relative to the SM for different Higgs boson masses ( $m_H$ ) as obtained by  $D\emptyset$ .

$m_H$ (GeV)	115	120	125	130	135	140	145	150	155	160	165	170	175	180	185	190	195	200
Expected	48.1	16.9	12.8	8.8	7.5	6.0	5.0	4.1	3.2	2.4	2.4	2.9	3.2	3.6	4.6	5.8	6.9	8.7
Observed	72.4	40.8	26.1	15.7	12.3	9.9	5.5	4.3	3.2	2.1	2.7	2.6	3.5	3.9	3.8	4.2	7.1	6.5

### 3.2. CDF Results on $p\bar{p} \rightarrow H \rightarrow WW$

In the  $2.4 \text{ fb}^{-1}$  CDF analysis [16], the events are triggered requiring different type of electromagnetic (EM) energy cluster for the electron based samples or track segments to record the muon based samples. Trigger efficiencies are measured using leptonic W and Z data samples. To improve the signal acceptance while maintaining acceptable background rejection for the  $W+$  jets and  $W\gamma$  processes where a jet or a  $\gamma$  is misidentified as a lepton, a lepton identification strategy similar to the one used in [17] is used. Candidate leptons are separated into six orthogonal sets: two for electrons; three for muons; and one for tracks that extrapolate outward to detector regions with insufficient calorimeter coverage for energy measurement. The two electron sets are central ( $|\eta| < 1.1$ ) using drift-chamber-based tracking, and forward ( $1.2 < |\eta| < 2.0$ ) using silicon-detector-based tracking. One of the muon set uses the muon chambers while the other two use tracks matched with energy deposits consistent with minimum ionization in the central or forward calorimeters. All lepton candidates are required to be isolated [16]. Candidate events are required to have exactly two lepton candidates. At least one lepton must match a trigger lepton candidate and have  $p_T > 20$  GeV, while the other one must have  $p_T > 10$  GeV.

Events are simulated with the MC@NLO program for WW [18], PYTHIA for the signal, Drell Yan,  $WZ$ ,  $ZZ$ , and  $t\bar{t}$ , and the generator described in [19] for  $W\gamma$ . The diboson backgrounds are suppressed in a similar way as in the  $D\emptyset$  analysis, with a specific treatment of the  $\cancel{E}_T$  [16], while the suppression of the  $t\bar{t}$  contribution is achieved by requiring fewer than two reconstructed jets with  $E_T > 15$  GeV and  $|\eta| < 2.5$  in the event. The  $W\gamma$  and  $W+$  jet backgrounds rejections are estimated from data.

After selection 661 events are observed while  $626 \pm 54$  background events are expected. The samples are then divided into high and low S/B classes. The dominant remaining background is  $WW$  production, and to separate it from the  $H \rightarrow WW$  signal two different multivariate techniques are combined, as in  $D\emptyset$ , i.e. a neural network approach using also Matrix Element discriminants, built as a Likelihood ratio ( $LR_{signal}$  of the event probabilities  $P_{signal}/[P_{signal} + \sum_i P_{background_i}]$ ). However, while  $D\emptyset$  is using only one  $LR$  with one signal ( $H \rightarrow WW$ ) and one main background ( $WW$  production), CDF builds several  $LR$ , assuming successively each important background as "signal". The final NN uses then six kinematic input variables, as shown in Figure 5 and five  $LR$ 's as shown in Figure 6. The resulting NN output is shown in Figure 6f for the high S/B case.

Since no excess is observed, limits are obtained using a Bayesian technique from the NN outputs, taking into account systematics uncertainties and their correlations as described in [16]. The resulting limits are given in Table III. These limits are compared to the ones obtained by  $D\emptyset$  in Figure 7.

Table III: Expected and observed upper limits at 95% CL for  $\sigma \times BR(H \rightarrow WW^{(*)})$  relative to the SM for different Higgs boson masses ( $m_H$ ) as obtained by CDF.

$m_H$ (GeV)	110	120	130	140	150	160	170	180	190	200
Expected	59.6	19.1	9.2	5.8	4.2	2.5	2.7	3.9	6.1	8.3
Observed	53.4	15.8	5.3	3.2	2.4	1.6	1.8	2.8	5.2	10.0



## 4. COMBINATION OF CDF AND DØ RESULTS

CDF and DØ have combined their most recent results on the searches for a SM Higgs boson produced in association with vector bosons ( $p\bar{p} \rightarrow WH \rightarrow \ell\nu b\bar{b}$ ,  $p\bar{p} \rightarrow ZH \rightarrow \nu\bar{\nu} b\bar{b}/\ell^+\ell^- b\bar{b}$  or  $p\bar{p} \rightarrow WH \rightarrow WW^+W^-$ ) or through gluon-gluon fusion ( $p\bar{p} \rightarrow H \rightarrow W^+W^-$ ) or vector boson fusion (VBF), in data corresponding to integrated luminosities ranging from 1.0-2.4fb<sup>-1</sup> at CDF and 1.1-2.3fb<sup>-1</sup> at DØ. In this combination the searches for Higgs bosons decaying to two photons or two tau leptons are added for the first time. The searches are separated into twenty nine mutually exclusive final states [20] referred to as “analyses” in the following. Integrated luminosities, and references to the collaborations’ public documentation for each analysis are given in Table IV for CDF and in Table V for DØ. The tables include the ranges of Higgs boson mass ( $m_H$ ) over which the searches were performed.

Table IV: Luminosity, explored mass range and references for the CDF analyses.  $\ell$  stands for either  $e$  or  $\mu$ .

	$WH \rightarrow \ell\nu b\bar{b}$	$ZH \rightarrow \nu\bar{\nu} b\bar{b}$	$ZH \rightarrow \ell^+\ell^- b\bar{b}$	$H \rightarrow W^+W^-$	$H + X \rightarrow \tau^+\tau^- + 2 \text{ jets}$
Luminosity (fb <sup>-1</sup> )	1.9	1.7	1.0	2.4	2.0
$m_H$ range (GeV/c <sup>2</sup> )	110-150	100-150	110-150	110-200	110-150
Reference	[21]	[22]	[23]	[24]	[25]

Table V: Luminosity, explored mass range and references for the DØ analyses.  $\ell$  stands for either  $e$  or  $\mu$ .

	$WH \rightarrow \ell\nu b\bar{b}$	$ZH \rightarrow \nu\bar{\nu} b\bar{b}$	$ZH \rightarrow \ell^+\ell^- b\bar{b}$	$H \rightarrow W^+W^-$	$WH \rightarrow WW^+W^-$	$H \rightarrow \gamma\gamma$
Luminosity (fb <sup>-1</sup> )	1.7	2.1	1.1	2.3	1.1	2.3
$m_H$ range (GeV)	105-145	105-145	105-145	110-200	120-200	105-145
Reference	[26]	[27]	[28]	[29],[30]	[31]	[32]

Several types of combinations, using the Bayesian and Modified Frequentist approaches, have been performed to ensure that the final result does not depend on the details of the statistical approach, and indeed, similar results (within 10%) have been obtained. Both methods rely on distributions in the final discriminants, and not just on their single integrated values. Systematic uncertainties enter as uncertainties on the expected number of signal and background events, as well as on the distribution of the discriminants in each analysis (“shape uncertainties”). Both methods use likelihood calculations based on Poisson probabilities. The Bayesian Method and Modified Frequentist method used are described in [20].

### 4.1. Systematic Uncertainties

Systematic uncertainties differ between experiments and analyses, and they affect the rates and shapes of the predicted signal and background in correlated ways. The combined results incorporate the sensitivity of predictions to values of nuisance parameters, and correlations are included, between rates and shapes, between signals and backgrounds, and between channels within experiments and between experiments. More on these issues can be found in [20] and in the individual analysis notes [21]-[32]. The main uncertainties are listed here below:

- **Correlated Systematics between CDF and DØ :** of the 6% uncertainty on the measurement of the integrated luminosity obtained by each experiment, 4% arises from the uncertainty on the inelastic  $p\bar{p}$  scattering cross section, which is correlated between CDF and DØ. The uncertainty on the production rates for the signal, for top-quark processes ( $t\bar{t}$  and single top) and for electroweak processes ( $WW$ ,  $WZ$ , and  $ZZ$ ) are taken as correlated between the two experiments. The uncertainties on the background rates for  $W/Z$ +heavy flavor are considered uncorrelated, as both CDF and DØ estimate these rates using data control samples, but employ different techniques. Other data driven uncertainty determinations (multijet, fake lepton or  $b$ -id rates) are taken uncorrelated between the two experiments for the same reason.
- **Correlated Systematic Uncertainties for CDF:** for  $H \rightarrow b\bar{b}$ , the largest uncertainties on signal arise from a scale factor for  $b$ -tagging (5.3-16%), jet energy scale (1-20%) and MC modeling (2-10%). The shape dependence

of the jet energy scale,  $b$ -tagging and uncertainties on gluon radiation are taken into account for some analyses. For  $H \rightarrow W^+W^-$ , the largest uncertainty comes from MC modeling (5%). For simulated backgrounds, the uncertainties on the expected rates range from 11-40%, depending on the background.

- **Correlated Systematic Uncertainties for  $D\bar{O}$ :**  $H \rightarrow b\bar{b}$  analyses have an uncertainty on the  $b$ -tagging rate of 3-10% per jet, and also an uncertainty on the jet energy and acceptance of 6-9% (jet identification, energy calibration and resolution). For the high mass analyses, the largest uncertainties are associated with lepton measurement and acceptance. These values range from 2-11% depending on the final state. The largest contributing factor to all analyses is the uncertainty on cross sections for simulated background, and is 6-18%.

## 4.2. Combined Results

Before extracting the combined limits we study the distributions of the log-likelihood ratio (LLR) for different hypothesis, to check the expected sensitivity across the mass range tested. Figure 8a displays the LLR distributions for the combined analyses as a function of  $m_H$ . Included are the results for the background-only hypothesis ( $LLR_b$ ), the signal and background hypothesis ( $LLR_{s+b}$ ), and for the data ( $LLR_{obs}$ ). The shaded bands represent the 1 and 2 standard deviation ( $\sigma$ ) departures for  $LLR_b$ .

Using the combination procedures outlined in [20], we extract limits on SM Higgs boson production  $\sigma \times B(H \rightarrow X)$  in  $p\bar{p}$  collisions at  $\sqrt{s} = 1.96$  TeV. For a simpler comparison with the standard model we present our results in terms of the ratio of obtained limits to cross section in the SM, as a function of Higgs boson mass, for test masses for which both experiments have performed dedicated searches in different channels. A value of 1 would indicate a Higgs boson mass excluded at 95% C.L. The expected and observed 95% C.L. ratios to the SM cross section for the combined CDF and  $D\bar{O}$  analyses are shown in Figure 8b. The observed and median expected limit ratios are given in Table VI, with observed (expected) values of 3.7 (3.3) at  $m_H = 115$  GeV and 1.1 (1.6) at  $m_H = 160$  GeV.

These results represent about a 40% improvement in expected sensitivity over those obtained on the combinations of results of each single experiment, which yield observed (expected) limits on the SM ratios of 5.0 (4.5) for CDF and 6.4 (5.5) for  $D\bar{O}$  at  $m_H = 115$  GeV, and of 1.6 (2.6) for CDF and 2.2 (2.4) for  $D\bar{O}$  at  $m_H = 160$  GeV.

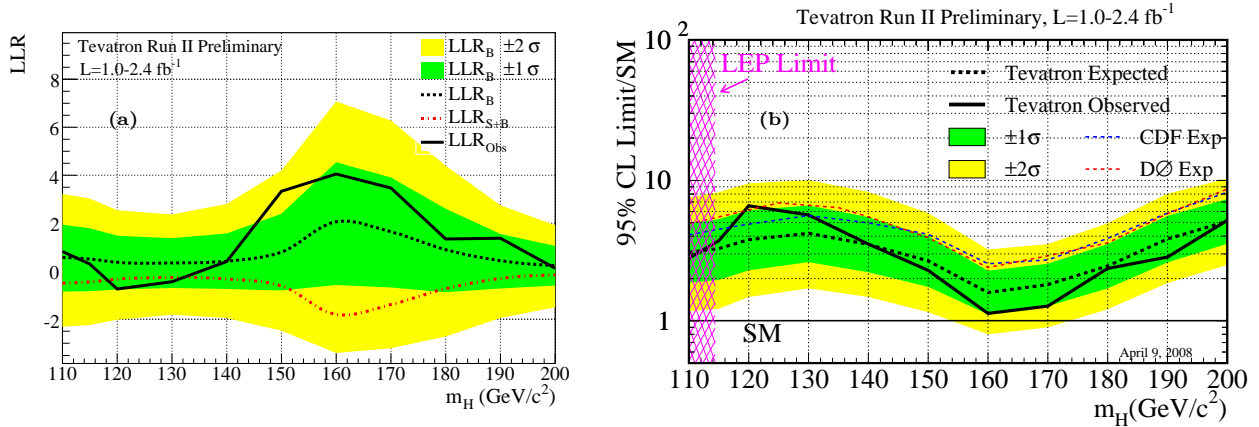


Figure 8: a) Log-Likelihood-Ration (LLR) plot for the CDF- $D\bar{O}$  combination, see [14] for more details; b) ratio to the SM Higgs production cross section of the 95% C.L. limit obtained with the combined CDF- $D\bar{O}$  analyses; the bands indicate the 68% and 95% probability regions where the limits can fluctuate, in the absence of signal; also shown are the expected upper limits obtained for all combined CDF channels, and for all combined  $D\bar{O}$  channels.



Table VI: Median expected and observed 95% CL cross section ratios for the combined CDF and  $D\bar{O}$  analyses as a function of the Higgs boson mass in GeV.

$m_H$ (GeV)	110	115	120	130	140	150	160	170	180	190	200
Expected	3.1	3.3	3.8	4.2	3.5	2.7	1.6	1.8	2.5	3.8	5.1
Observed	2.8	3.7	6.6	5.7	3.5	2.3	1.1	1.3	2.4	2.8	5.2

## 5. PROSPECTS

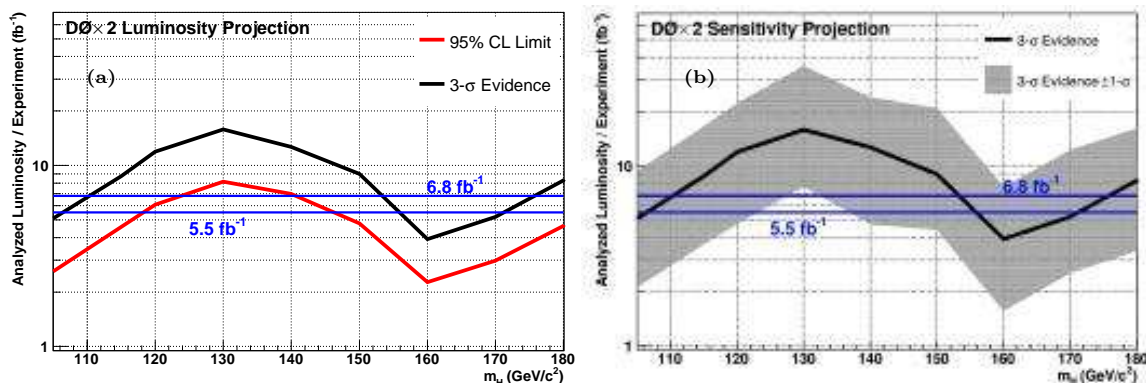


Figure 9: Prospect for Higgs search sensitivity at the Tevatron assuming the analysis improvements described in the text and similar performance between CDF and  $D\bar{O}$  analyses. The two horizontal lines correspond to a running until 2009 and 2010.

In Fall 2007, the two collaborations were asked to review their prospects for Higgs sensitivity in case of a 2009 or a 2009+2010 running of the Tevatron. Looking back, since 2005, the high mass experimental sensitivity for the Higgs has improved by a factor of 1.7 (without counting the gain due to luminosity) and this was mainly due to improvements with multivariate techniques and with lepton acceptance. From 2007 to 2010,  $D\bar{O}$  estimated a possible additional improvement in analysis sensitivity by a factor of 1.4, coming from increased lepton efficiency (10% per lepton) and further multivariate analyses improvements (30% in sensitivity). Other potential improvements (like the inclusion of tau channels) were not included in the estimate. CDF estimates were similar, so we could effectively estimate the Tevatron potential independently and both experiments reached similar conclusions.

At low mass, since 2005, the analyses sensitivities have also improved by a factor of approximately 2, due to increase in acceptance, kinematic phase space, trigger efficiency, asymmetric tagging for double b-tags, b-tagging improvements (NN b-tagging), and improved statistical techniques/event NN discriminant. From 2007 to 2010, we estimated that we will gain an additional factor of 2.0 beyond the improvement expected from the increased luminosity: b-tagging improvements, di-jet mass resolution, increased lepton efficiency, improved multivariate techniques.

With such improvements, we obtain the 95% C.L. and  $3\sigma$  sensitivity curves given in Figure 9a as a function of the analyzed data. The predicted delivered luminosity from the Tevatron when adding a 2010 running is  $8\text{ fb}^{-1}$ , resulting in  $6.8\text{ fb}^{-1}$  of high quality analyzed data, as shown in the Figure. With the data accumulated by the end of 2010, the combined data of the CDF and  $D\bar{O}$  experiments could allow to explore much of the SM Higgs mass region allowed by the precision electroweak measurements. Three-sigma evidence for a Higgs is possible over almost the entire range, as can be seen from the  $1\text{-}\sigma$  band in Figure 9b, and is probable for the low and high end of this mass spectrum if the Higgs boson lies there. The low mass searches are particularly important, since the Tevatron and LHC would be searching for it in different decay modes ( $H \rightarrow b\bar{b}$  at the Tevatron,  $H \rightarrow \gamma\gamma$  at the LHC).

In conclusion, the search for the SM Higgs boson has reached a mature state at the Tevatron, the combination techniques are in place, and the analyses are continuing to improve their individual sensitivity such that the Tevatron combination would reach SM Higgs sensitivity between 115 and 185 GeV by the end of Run II.

## Acknowledgments

The author wish to thank the organizers for a stimulating conference, and all the CDF and DØ colleagues for the results obtained together and presented here.

## References

- [1] R. Barate *et al.*, Phys. Lett. B **565**, 61 (2003).
- [2] The LEP Electroweak Working Group, arXiv:0712.0929 [hep-ex].
- [3] R. Hughes, for the CDF and DØ collaboration, these proceedings.
- [4] CDF Collaboration, CDF-Note 7307 (2008)
- [5] DØ Collaboration, DØ -Note 5485 (2007)
- [6] DØ Collaboration, Phys. Rev. Lett. **97**, 151804 (2006).
- [7] DØ Collaboration, DØ -Note 5624 (2008)
- [8] T. Sjostrand, S. Mrenna, and P. Skands, J. High Energy Phys. 0605, 026 (2006).
- [9] M.L. Mangano, M. Moretti, F. Piccinini, R. Pittau, A. Polosa, JHEP 0307:001,2003, hep-ph/0206293.
- [10] J. Pumplin *et al.*, J. High Energy Phys. 07 (2002) 012.
- [11] R. Hamberg, W.L. van Neerven, and T. Matsuura, Nucl. Phys. **B359**, 343 (1991) [Err.-ibid.**B644**, 403 (2002)].
- [12] J. M. Campbell and R. K. Ellis, Phys. Rev. D **60**, 113006 (1999).
- [13] T. Junk, Nucl. Instrum. Methods Phys. Res. A. **434**, 435 (1999). A. Read, CERN 2000-005 (30 May 2000).
- [14] W. Fisher, FERMILAB-TM-2386-E.
- [15] DØ Collaboration, DØNote 5537 (2007)
- [16] CDF Collaboration, CDF-Note 9236 (2008)
- [17] CDF Collaboration, Phys. Rev. Lett. **98**, 161801 (2007).
- [18] S. Frixione and B. R. Webber, J. High Energy Phys.0206, 029 (2002).
- [19] U. Baur and E. L. Berger, Phys. Rev. D **47**, 4889 (1993).
- [20] CDF and DØ Collaborations, “Combined CDF and DØ Upper Limits on Standard Model Higgs-Boson Production”, FERMILAB-PUB-07-656-E, arXiv:0712.2383
- [21] CDF Collaboration, ”Search for Higgs Production in Association with W Boson with  $1.7 \text{ fb}^{-1}$ ”, CDF Note 8957.
- [22] CDF Collaboration, “Search for the SM Higgs Boson in the Missing Et and B-jets Signature”, CDF Note 8973.
- [23] CDF Collaboration, “Search for ZH in  $1 \text{ fb}^{-1}$ ”, CDF Note 8742.
- [24] CDF Collaboration, “Search for  $H \rightarrow WW$  production using  $1.9 \text{ fb}^{-1}$ ”, CDF Note 8923.
- [25] CDF Collaboration, “Search for SM Higgs using tau leptons using  $2 \text{ fb}^{-1}$ ”, CDF Note 9179.
- [26] DØ Collaboration, “Search for WH Production at  $\sqrt{s} = 1.96 \text{ TeV}$  with Neural Networks,” DØ Note 5472.
- [27] DØ Collaboration, “Search for the standard model Higgs boson in the  $HZ \rightarrow b\bar{b}\nu\nu$  channel in  $2.1 \text{ fb}^{-1}$  of ppbar collisions at  $\sqrt{s} = 1.96 \text{ TeV}$ ”, DØ note 5586.
- [28] DØ Collaboration, “A Search for  $ZH \rightarrow \ell^+\ell^-b\bar{b}$  Production at DØ in  $p\bar{p}$  Collisions at  $\sqrt{s} = 1.96 \text{ TeV}$ ”, DØ Note 5482.
- [29] DØ Collaboration, “Search for the Higgs boson in  $H \rightarrow WW^* \rightarrow l^+l^- (\ell, \ell' = e\mu)$  decays with  $1.7 \text{ fb}^{-1}$  at DØ in Run II”, DØ Note 5537.
- [30] DØ Collaboration, “Search for the Higgs boson in  $H \rightarrow WW^*$  decays with  $1.2 \text{ fb}^{-1}$  at DØ in Run IIB”, DØ Note 5624.
- [31] DØ Collaboration, “Search for associated Higgs boson production  $WH \rightarrow WWW^* \rightarrow \ell^\pm\nu\ell'^\pm\nu' + X$  in  $p\bar{p}$  collisions at  $\sqrt{s} = 1.96 \text{ TeV}$ ”, DØ Note 5485.
- [32] DØ Collaboration, “Search for a light Higgs boson in  $\gamma\gamma$  final state”, DØ Note 5601.
- [33] CDF Collaboration, “Combined Upper Limit on Standard Model Higgs Boson Production”, CDF Note 8941.
- [34] DØ Collaboration, “Combined upper limits on standard model Higgs boson production from the D0 experiment with  $1.1\text{-}2.4 \text{ fb}^{-1}$ ” DØ Note 5625.